The effect of magnetic order and thickness in the Raman spectra of oriented thin films of $LaMnO_3$

2007 J. Phys.: Condens. Matter 19 346232

(http://iopscience.iop.org/0953-8984/19/34/346232)

IOP PUBLISHING JOURNAL OF PHYSICS: CONDENSED MATTER

J. Phys.: Condens. Matter **19** (2007) 346232 (10pp) doi:10.1088/0953-8984/19/34/346232

The effect of magnetic order and thickness in the Raman spectra of oriented thin films of $LaMnO_3$

Aditi Dubey and V G Sathe[1]

UGC-DAE Consortium for Scientific Research, University Campus, Khandwa Road, Indore-452 017, India

E-mail: vasant@csr.ernet.in

Received 2 May 2007, in final form 4 July 2007
Published 31 July 2007
Online at stacks.iop.org/JPhysCM/19/346232

Abstract

Low-temperature Raman studies on (100)-oriented $LaMnO_3$ thin films of different thicknesses deposited on $LaAlO_3$(100) substrate by using the pulsed laser deposition technique are presented. The phonon mode frequencies depend strongly on the thickness of the film and in comparison to the $LaMnO_3$ single crystal shift to higher values with decreasing thickness. The broadening of Raman line widths was also observed with decreasing film thickness. Anomalous softening of the B_{2g} mode (Jahn–Teller distortion activated) was observed for all films below the magnetic ordering temperature. A signature of lattice anomalies in the form of changes in line width of the B_{2g} mode correlated with the magnetic ordering temperature was also seen. The results were interpreted by considering strong spin–phonon coupling and reduction in Jahn–Teller distortion driven polarons due to magnetic order.

(Some figures in this article are in colour only in the electronic version)

1. Introduction

The discovery of colossal magnetoresistance of members of the manganite system has opened up their many technological applications [1, 2]. In manganite physics, the parent compound, $LaMnO_3$, is of particular importance. This compound undergoes a phase transition from the low-temperature A-type antiferromagnetic (AFM) insulator orbital ordered (OO) phase to the paramagnetic phase at ∼140 K to the orbital disordered phase above ∼780 K [1, 3–5]. However, the non-stoichiometric compounds $LaMnO_{3\pm\delta}$ show properties that match doped $LaMnO_3$ [6]. They show a ferromagnetic–metallic contribution that depends on the extent of the oxygen stoichiometry.

Pulsed laser deposition (PLD) has been extensively used to produce good-quality oriented/epitaxial thin films of desired thickness. The physical properties of thin films can be tailored by controlling the growth conditions. Because of the subtle balance between

[1] Author to whom any correspondence should be addressed.

several competing phases, a small change in oxygen occupancies can lead to drastic changes in their physical properties. However, controlling the oxygen stoichiometry is still a very challenging task and often films with non-stoichiometry result. Aruta *et al* [7] reported the effect of oxygen content on the structural properties of $LaMnO_3$ films and optimized the oxygen pressure during deposition to get perfectly stoichiometric thin films by PLD. Jin *et al* [8] performed the first systematic experimental study of the effect of thickness on the magneto-transport properties of thin films, which was later followed by others [9]. Recently, it has also been realized that strain fields due to lattice mismatch, lattice distortion has a large effect on charge order (CO) formation and CO can induce a lattice distortion through the electron–lattice interaction manifested by the Jahn–Teller effect [10, 11]. Furthermore, it has been shown by many workers that spin–lattice coupling [12, 13] plays an important role in determining the transport properties of these compounds. One of the most important features peculiar to manganite thin films is the close relationship between the electronic, transport and magnetic properties and the strain effect induced by the substrate. In fact the magnetoresistance response (MR), the semiconductor to metallic-like transition temperature (T_{S-M}) and the paramagnetic–ferromagnetic transition temperature (T_c) can be nicely tuned by controlling the film thickness and the substrate nature.

Raman spectroscopy is most frequently used for characterizing the lattice-vibrational properties. It is also used to elucidate the spin–phonon and electron–phonon interaction present in the system. Raman data for various $RE_{1-x}A_xMnO_3$ (RE = rare earths) series of compounds and an assignment for most of the phonons that appear have been proposed [14–16]. Some low-temperature Raman studies of oriented manganite thin films of doped compounds have also been reported [17–19]. It has been shown that the optical phonons, in particular those accessible by Raman spectroscopy, are sensitive to local lattice distortions. In previous studies of single crystals, it was found that Raman spectra of manganites usually contain three different comparable contributions: (i) sharp features that follow the selection rules for first-order Raman scattering, (ii) the relatively broad second-order scattering, (iii) those due to electronic scattering [20]. The non-stoichiometric films often show a metal–insulator transition and very large magnetoresistance (MR) [18]. Understanding the physics involved behind the large MR is crucial for all applications. The variation of Raman and/or infrared phonon spectra with magnetic ordering can help us to understand the interplay of structural and magnetic properties. This has been a very important issue in $RMnO_3$ compounds. However, apart from a few studies on bulk and single crystals, no results on thin film samples concerning the behaviour of Raman phonons across the magnetic ordering temperature in these undoped compounds are available [3, 14–24].

In this paper we present low-temperature Raman studies on different thicknesses of $LaMnO_3$ (LMO) thin films grown on $LaAlO_3$ (LAO) (100) substrate. Anomalous changes in the phonon frequencies and line widths are observed for all the films at low temperature that are attributed to spin–phonon and electron–phonon interactions.

2. Experimental details

Polycrystalline $LaMnO_3$ bulk compound was prepared by the standard solid-state reaction method of mixing stoichiometric amounts of precursors (purity of 99.9% from Aldrich) with intermediate grinding and sintering at 1350 °C several times. The polycrystalline sample was characterized by the x-ray diffraction (XRD) technique. A Rigaku powder diffractometer fitted on a rotating anode (18 kW) x-ray generator with a Cu target was used for measurements. The compound was found to be single phase in nature. The XRD pattern was refined by using the FullProf refinement program [25]. The pattern was fitted to the $R\bar{3}c$ space group and the lattice parameters thus obtained were $a = b = 0.552$ nm and $c = 1.13$ nm. LMO

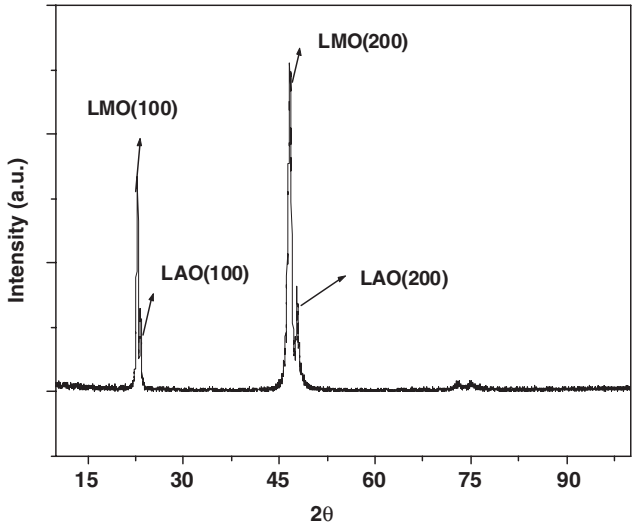

Figure 1. X-ray diffraction pattern of $LaMnO_{3\pm\delta}$ film of ∼50 nm thickness deposited on $LaAlO_3$ substrate across the (100) and (200) reflections of $LaMnO_3$ film and $LaAlO_3$ substrate.

films of different thickness were prepared by using the pulsed laser deposition technique with an excimer laser with wavelength $\lambda = 248$ nm. The substrate temperature was kept at ∼650 °C in 300 mTorr oxygen (O_2) pressure. After deposition the films were annealed for 15 min at the same O_2 pressure and for 15 min in vacuum. The structure of the films was characterized by XRD. The thickness of the films was measured with the help of an XP1 telystep profilometer. Raman spectra were collected in backscattering geometry using a He–Ne excitation source having wavelength 632.81 nm coupled with a Labram-HR800 microRaman spectrometer equipped with a 50× objective, appropriate notch filter and a Peltier cooled charge-coupled device detector. For the low-temperature Raman measurements, the sample was mounted on a THMS600 stage from Linkam UK. During the low-temperature measurements, in the present experimental set up a 1800 g mm^{-1} grating is used in high-resolution dispersive geometry. In order to achieve very high positional accuracy the grating was kept unmoved during the entire temperature scan. A spectral window of ∼325 cm^{-1} was covered with a positional accuracy of 0.33 cm^{-1} in such a configuration. The Raman frequencies and Raman line widths were obtained from the best fit to the Lorentzian line shape after baseline correction.

3. Results

Figure 1 shows the typical XRD pattern for a $LaMnO_3$ film of ∼50 nm thickness recorded from 10° to 100°. Two highly intense diffraction peaks corresponding to (100) and (200) indices of the pseudo-cubic unit cell of the $LaMnO_3$ film are seen along with substrate peaks of the same orientation. No other peak apart from the (h00) peaks of the film and substrate were observed. The other two films having thickness of about ∼200 and ∼150 nm also showed similar x-ray diffraction patterns with small changes in peak position. From this we conclude that all the films are single phase, highly oriented and of very good quality. In thin films it is rather very difficult to distinguish between rhombohedral $R\bar{3}c$ and orthorhombic *Pnma* structures from x-ray diffraction studies. The pseudo-perovskite lattice parameters of the orthorhombic unit cell of $LaMnO_3$ are typically $a_1 = a_2 = 0.398$ nm and $a_3 = 0.385$ nm. In strained

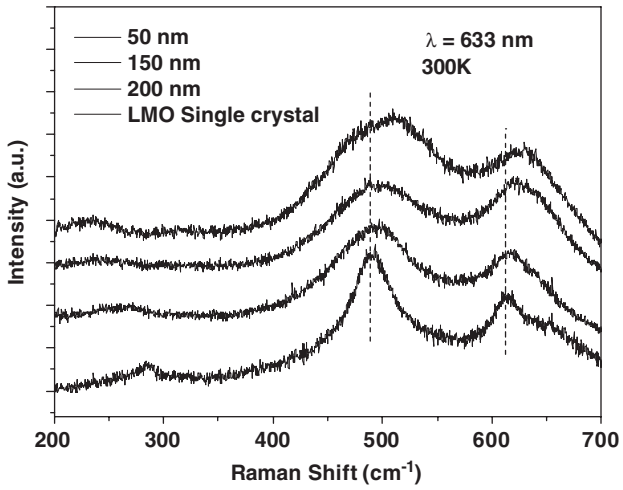

Figure 2. Room-temperature (300 K) Raman spectra of $LaMnO_3$ films of thickness 200, 150, 50 nm and a single crystal of $LaMnO_3$ ($\lambda = 632.81$ nm).

film the in-plane lattice parameters are compressed to match the substrate, yielding a pseudo-cubic unit cell. Other studies on these films, not reported here, suggest that the films are non-stoichiometric in nature. Generally, the non-stoichiometric $LaMnO_3$ compounds often show an orthorhombic structure at and below room temperature [26]. We therefore assumed that the films are orthorhombic in nature, with the *Pnma* space group.

In figure 2, room-temperature Raman spectra for LMO films having thickness ∼200, ∼150 and ∼50 nm excited by the 632.81 nm laser line are shown in the frequency interval 200–700 cm^{-1}. For comparison, the Raman spectrum of a $LaMnO_3$ single crystal is also shown. The individual spectrum is shifted vertically for the sake of clarity. In an ideal cubic ABO_3 perovskite, all atoms are at centrosymmetric sites and hence do not contribute to Raman modes. In the orthorhombic *Pnma* (D_{2h}^{16}) structure, the atoms occupy four non-equivalent atomic sites (RE, Mn, O_1, and O_2); of these only the Mn site is at a centre of symmetry. The distortion caused due to the motions of oxygen atoms in Mn–O_6 octahedra around the Mn ion are responsible for the Raman active vibrations. Group theoretical analysis of the site symmetries of this compound shows that there are 60 Γ-point phonon modes in the orthorhombic $LaMnO_3$ compound. Only 24 of them ($7\ A_g + 5\ B_{1g} + 7\ B_{2g} + 5\ B_{3g}$) are Raman active [13, 23, 24]. Several weak Raman bands along with two most prominent Raman bands ($\omega_1 \sim 490$ cm^{-1} and $\omega_2 \sim 608$ cm^{-1}) were observed in the room-temperature spectra (figure 2). The positions and widths of observed Raman modes match well with the orthorhombic structure [14, 23]. According to Iliev *et al* [23], the Raman mode ω_1 centred around ∼490 cm^{-1} belongs to A_g symmetry and corresponds to the O_2 antistretching and MnO_6 bending. The other mode at ω_2 centred around ∼608 cm^{-1} is of B_{2g} symmetry that originates from the 'Jahn–Teller distortion'. The band positions and line widths of the A_g and B_{2g} Raman bands resulting from the fit using multiple Lorentzian functions are listed in table 1. A representative curve showing the Lorentzian fitting is shown in figure 3, along with the fitting results. A close look at the table shows that the Raman mode positions shift towards higher frequency as compared to bulk single crystal, and the corresponding widths also increase with decreasing film thickness. The Raman studies show a remarkable difference in the phonon frequencies with thickness. This behaviour can be explained on the basis of the strain accommodated on different films

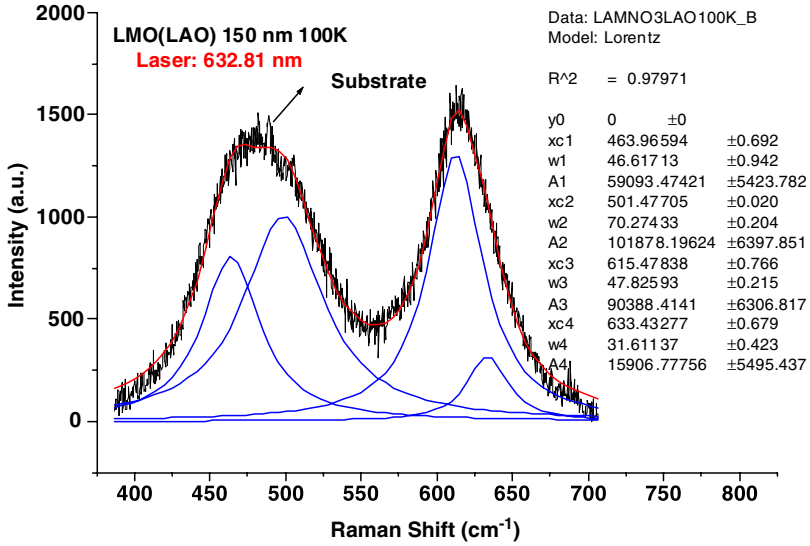

Figure 3. Representative Raman spectrum of a $LaMnO_3$ film of 150 nm thickness (100 K) fitted by using Lorentzian functions.

Table 1. Room-temperature Raman peak positions of a $LaMnO_3$ single crystal and films of different thicknesses (200, 150 and 50 nm).

Sample	A_g mode position (cm^{-1})	A_g line width (cm^{-1})	B_{2g} mode position (cm^{-1})	B_{2g} line width (cm^{-1})
LMO single crystal	487.05	29.34	608.70	18.52
200 nm	493.64	81.92	617.66	56.46
150 nm	494.72	86.7	623.02	60.26
50 nm	497.63	107.38	624.03	74.89

due to lattice mismatch and increase in the lattice distortion with decreasing thickness. As the thickness is increased the strain is released and the Raman frequencies appear close to the phonon frequencies of the single crystal. From the XRD studies it was inferred that the thickness effects leading to strain are negligible after ∼100 nm [29]. However, the present study shows that the Raman frequencies are different for 150 and 200 nm films. This shows that Raman measurements are more sensitive than XRD to the thickness (strain) related effects.

4. Low-temperature Raman study

Low-temperature measurements were carried out for 150, 50 nm thick films and a single crystal of $LaMnO_3$. Figure 4 shows typical low-temperature Raman spectra collected from ∼300 to ∼725 cm^{-1} for LMO film of thickness ∼150 nm from 300 K down to 90 K at selected temperatures. The intensity of the two strongest Raman bands, namely A_g and B_{2g} centred around ∼490 and ∼608 cm^{-1} gradually enhanced on lowering temperature. As mentioned before the exact peak positions and line widths were extracted from fitting the bands by Lorentzian function. The error bars obtained in the fitting procedure are at the most ±0.7 cm^{-1} for both Raman band position and bandwidth and are comparable with the size of the symbols used in the plots (figures 5 and 6).

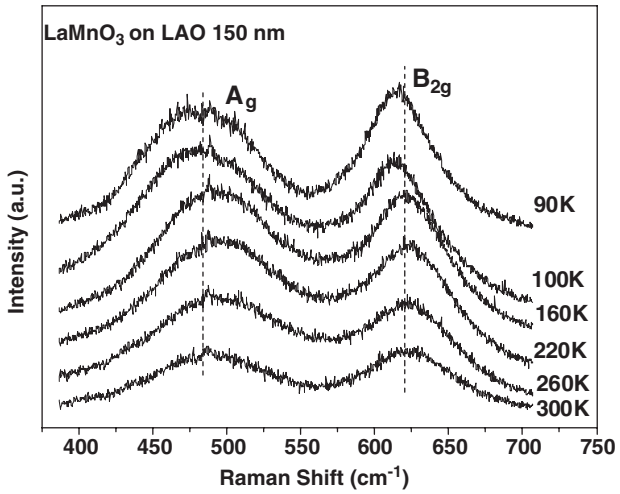

Figure 4. Low-temperature Raman spectra for $LaMnO_3$ film of ∼150 nm thickness at selected temperatures recorded from 300 K down to 90 K.

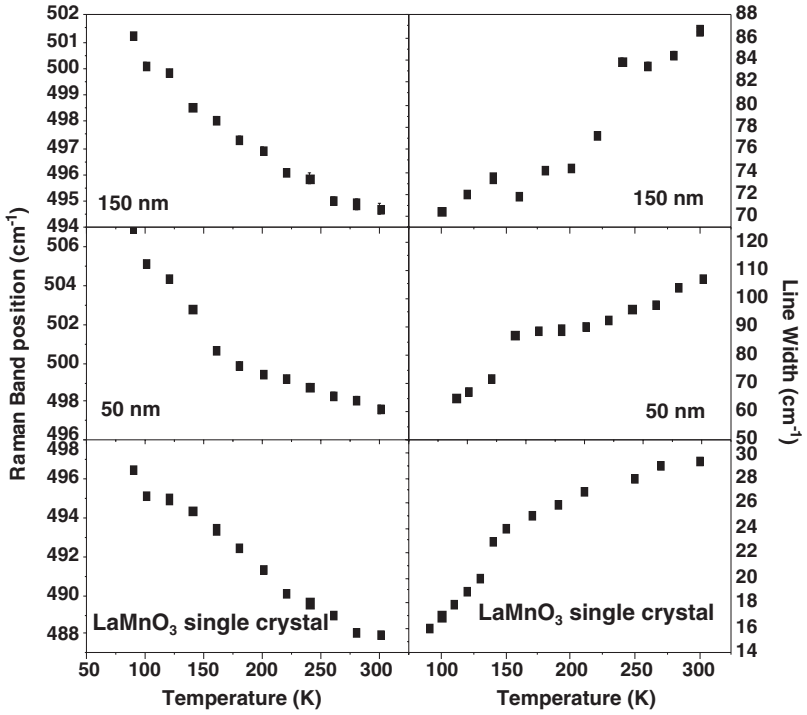

Figure 5. Temperature-dependent A_g mode position (left-hand side) and line width (right-hand side) behaviour of $LaMnO_3$ films of thicknesses ∼150 nm and ∼50 nm and a $LaMnO_3$ single crystal respectively. The error bars are less than or comparable to the size of the symbols used.

In figure 5, the temperature evolution of the Raman band frequency (left-hand side) of the A_g mode along with the line widths (right-hand side) is plotted for the two films and single crystal. Observation of the figure shows that the A_g mode exhibits normal hardening and a

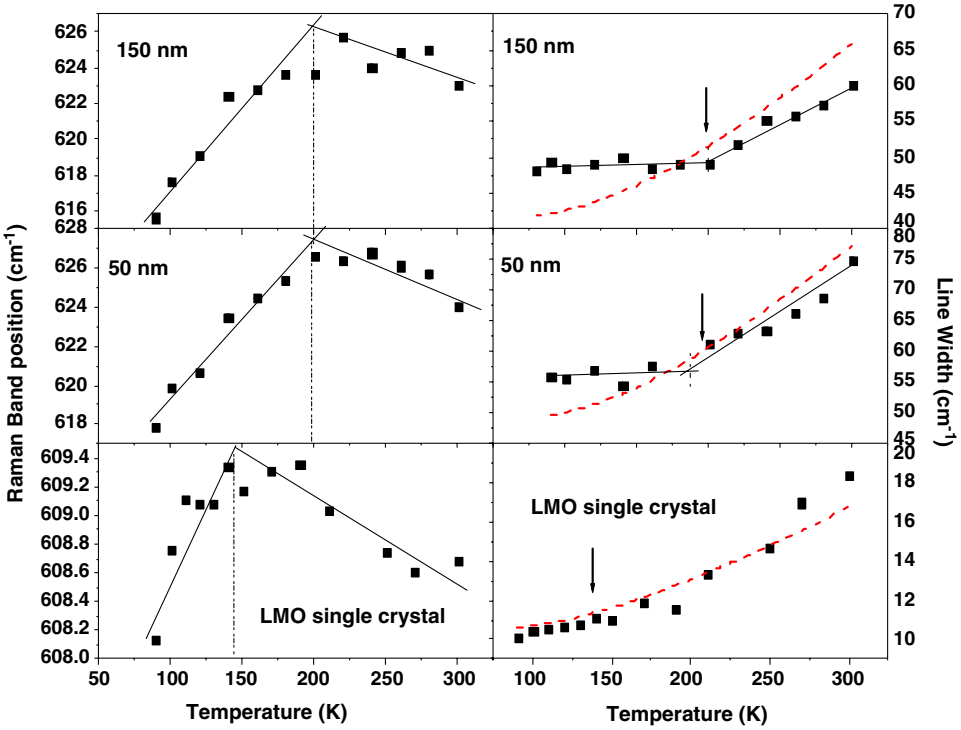

Figure 6. Temperature-dependent B_{2g} mode position (left-hand side) and line width (right-hand side) behaviour of films having thickness ∼150 nm, ∼50 nm and a $LaMnO_3$ single crystal respectively. Straight lines in the left column are guide to eyes. The dashed lines in the right columns are simulated curves fitted by an anharmonic model. The arrow depicts the magnetic transition temperature. The error bars are less than or comparable to the size of the symbols used.

decrease in the line width with decreasing temperature. Raman band hardening with lowering temperature is attributed to lattice contraction and anharmonic effects.

The temperature dependence of the B_{2g} mode position (left-hand side) and corresponding line widths (right-hand side) is shown in figure 6 for all the samples. It is clear from the figure that the B_{2g} mode frequency first hardens and then, below a critical temperature, it starts decreasing as the temperature is lowered. As depicted by the dashed line, the anomalous softening of the frequency starts at ∼140 K for the single crystal. It is interesting to note that for the stoichiometric $LaMnO_3$ sample an antiferromagnetic transition is reported around this temperature [16, 28]. For thin films, the softening of the B_{2g} mode frequency for ∼150 and ∼50 nm thick films starts around ∼200 K. The corresponding plot for line widths of the B_{2g} mode as a function of temperature for films also shows anomalous behaviour. The width shows a sharp decrease with lowering temperature until ∼200 K and then changes slope. However, for the single crystal such a drastic change in slope is not seen and the behaviour as a function of temperature can be fitted with the anharmonic model [27] function for the full width at half maximum (FWHM):

$$\Gamma(T) = A\left[1 + \frac{2}{e^x - 1}\right]$$

where A is a constant and $x = \frac{\hbar\omega_0}{2k_B T}$, ω_0 is the Raman frequency and T is the temperature in kelvin. The simulated curve for $\omega_0 = 610\ \text{cm}^{-1}$ and $A = 10.43$ is shown by a dashed line.

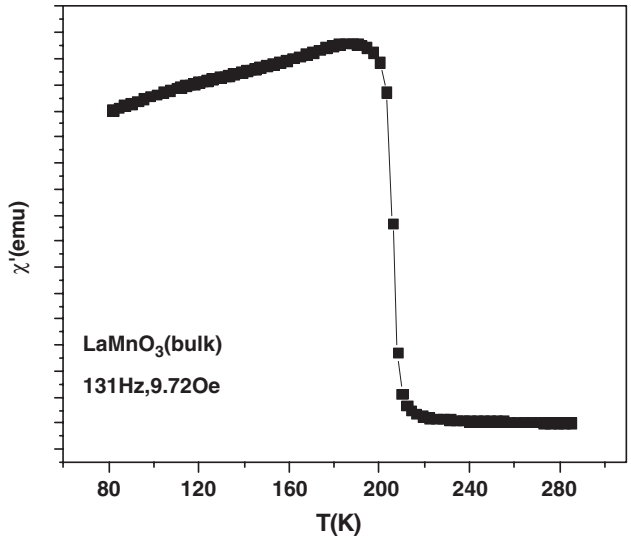

Figure 7. AC susceptibility of $LaMnO_3$ polycrystalline bulk compound as a function of temperature.

Similarly, simulated curves for films are also shown. It is clear from the figure that for films the function deviates a lot from its expected behaviour below the magnetic ordering temperature depicted by an arrow.

Figure 7 shows the magnetic susceptibility behaviour as a function of temperature for polycrystalline bulk $LaMnO_{3\pm\delta}$ compound. This same compound was used as a target during thin film deposition. The susceptibility shows a drastic change below 207 K, which is a signature of the occurrence of magnetic order. Normally for non-stoichiometric compounds ($LaMnO_{3\pm\delta}$ $\delta > 0$) this transition is attributed to ferromagnetic order [6, 24].

It is worth mentioning here that the temperature below which the Raman frequency shows softening and the line width shows a slope change in thin films was close to the magnetic ordering temperature.

5. Discussion

Iliev and Abrashev [16] argued that strong high-wavenumber phonons observed between 400–700 cm^{-1} are not proper Raman modes for $R\bar{3}c$ or *Pnma* structures. Rather, these modes are of phonon density of states origin and correspond to oxygen phonon branches activated by the non-coherent Jahn–Teller (JT) distortion of the Mn^{3+}–O_6 octahedra. They further argued that these modes disappear in the ferromagnetic metallic phase. The non-coherent JT distortions can be either small or large. Small lattice perturbations will affect mainly the phonon lifetime, thus causing line broadening in the phonon frequencies. In the present study the line widths for single-crystal $LaMnO_3$ (table 1) are not very large and they show monotonic behaviour across the magnetic transition. This indicates that the JT distortion is large. However, unlike previous findings [16], in the present study a clear signature of antiferromagnetic (AFM) order in the form of softening of the B_{2g} mode in the single-crystal sample is seen. The A_g mode on the other hand shows normal hardening as the temperature is lowered below the magnetic ordering temperature. Granado *et al* [13] observed softening of B_{2g} mode across the AFM ordering in $LaMnO_3$ and attributed it to the changes in the lattice parameters at

T_N. In another report, Granado *et al* [24] showed that the amount of softening of the B_{2g} mode depends very much on the amount of excess oxygen (δ) present in $LaMnO_{3\pm\delta}$ samples. The softening of the mode across the magnetic transition decreases as δ increases. From a comparison with lattice parameters it was argued that anharmonic and magnetostriction effects do not play any role in the softening of the phonon mode. From the theoretical expressions it was shown that spin–phonon coupling is mainly responsible for the observed softening. In this model only super-exchange coupling between Mn^{3+} ions is considered, and double exchange and Dzyaloshinsky–Moriya interactions are neglected. However, in the present study we find that softening is observed for all the samples, whether antiferromagnetic with perfect stoichiometry ($\delta = 0$) single crystal or non-stoichiometric thin films with $\delta \neq 0$ showing a ferromagnetic transition around 200 K (figure 6). The softening temperature is in the vicinity of the magnetic ordering temperature in all the films. The other feature worth noticing is the anomalous change in the line width of the B_{2g} mode seen in all the films with ferromagnetic contributions and its absence in the single-crystal sample with antiferromagnetic interactions. The line width shows a change in slope at the magnetic ordering temperature in thin film samples. This strongly indicates that the ferromagnetic order in followed by an order–disorder type of transition [22]. In the polaron driven transport model [27] this suggests a possible transition from small-polaron to large-polaron activated behaviour. Small and large polarons are manifestations of short-range and long-range lattice distortion that is coupled with magnetic order, causing changes in the line width broadening. Thus it is appropriate to consider both the mechanisms for anomalous softening of the B_{2g} mode: (i) strong spin–phonon coupling and (ii) polaron-activated effects, which reduce the JT distortion [23] below the magnetic ordering temperature, inducing softening and changes in the line width broadening.

In summary, we have carried out a systematic low-temperature Raman study of non-stoichiometric $LaMnO_{3\pm\delta}$ thin films of different thickness deposited on $LaAlO_3$(100) substrate by pulsed laser deposition. For comparison, similar studies on a stoichiometric single crystal were also performed. The B_{2g} mode centred around $\sim$608 cm^{-1} shows anomalous softening in all the thin films and the single crystal when cooled down below the magnetic ordering temperature. The anomalous softening of frequency is accompanied with a change in line width broadening near the ferromagnetic ordering temperature for non-stoichiometric thin film samples. The stoichiometric single crystal showed normal behaviour as far as line width is concerned. The results were interpreted by considering the presence of strong spin–phonon interactions and reduction in JT distortion driven polarons due to ferromagnetic ordering.

Acknowledgments

The authors would like to acknowledge Dr P Chaddah for constant encouragement and support. They would also like to thank Dr R J Choudhary for x-ray diffraction measurements and Mr Ashim Pramanik and Dr A Banerjee for help in magnetic susceptibility measurements. AD is grateful to the Council for Scientific and Industrial Research, New Delhi, for financial support.

References

[1] Murakami Y, Hill J P, Gibbs D and Blume M 1998 *Phys. Rev. Lett.* **81** 582
[2] Tokura Y and Tomioka Y 1999 *J. Magn. Magn. Mater.* **200** 1 and references therein
Coey J M, Verit M and von Molenar S 1999 *Adv. Phys.* **48** 167 and references therein
[3] Zhou J S and Goodenough J B 1999 *Phys. Rev.* B **60** R15002
[4] Chatterji T, Fauth F and Ouladdiaf B 2003 *Phys. Rev. Lett.* **68** 52406
[5] Zenia H, Gehring G A and Temmerman W M 2005 *New J. Phys.* **7** 257

[6] Subias G, Garcia J, Blasca J and Proietti M G 1998 *Phys. Rev.* B **58** 9287
[7] Aruta C, Angeloni M and Balestrino G 2006 *J. Appl. Phys.* **100** 023910
[8] Jin S, Tiefel T H, McCormack M and O'Bryan H M 1995 *Appl. Phys. Lett.* **67** 557
[9] Sun J Z, Abraham D W, Rao R A and Eom C B 1999 *Appl. Phys. Lett.* **74** 3017
[10] Tao J and Zuo J M 2004 *Phys. Rev.* B **69** 180404
[11] Loudon J C and Midgley P A 2005 *Phys. Rev.* B **71** 220408
[12] Podobedov V B, Waber A, Romero D B, Rice J P and Drew H D 1998 *Phys. Rev.* B **58** 43
[13] Granado E, García A, Sanjurjo J A, Rettori C and Torriani I 1998 *Phys. Rev.* B **58** 11435
[14] Iliev M N and Abrashev M V 1998 *Phys. Rev.* B **57** 2872
[15] Abrashev M V, Litvinchuk A P, Iliev M N and Mang R L 1999 *Phys. Rev.* B **59** 4146
[16] Iliev M N and Abrashev M V 2001 *J. Raman Spectrosc.* **32** 805
[17] Tatsi A, Papadopoulou E L and Lampakis D 2003 *Phys. Rev.* B **68** 24432
[18] Xiong Y M, Chen T, Wang G Y and Chen X H 2004 *Phys. Rev.* B **70** 94407
[19] Choi K Y, Lemmens P and Sahaoui T 2005 *Phys. Rev.* B **71** 174402
[20] Podobedov V B, Romero D B, Waber A and Rice J P 1998 *Appl. Phys. Lett.* **73** 3217
[21] Cochram W 1961 *Adv. Phys.* **9** 387
Cochram W 1960 *Adv. Phys.* **10** 401
[22] Houssion E 1998 *Key Eng. Mater.* **155** 1
[23] Iliev M N, Abrashev M V, Laverdière J, Jandl S, Gospodinov M M, Wang Y Q and Sun Y Y 2006 *Phys. Rev.* B **73** 064302
[24] Granado E, García A, Sanjurjo J A, Rettori C and Torriani I 1999 *Phys. Rev.* B **60** 11879
[25] Rodríguez-Carvajal J 1993 *Physica* B **192** 55
[26] Ritter C, Ibarra M R, De Teresa J M and Algarabel P A 1997 *Phys. Rev.* B **56** 8902
Huang Q, Santoro A and Lynn J W 1997 *Phys. Rev.* B **55** 14987
[27] Balkanski M, Wallis R F and Haro E 1983 *Phys. Rev.* B **28** 1928
[28] Allen P B and Perebeinos V 1999 *Phys. Rev. Lett.* **83** 4828
[29] Dore P, Funaro A, Sacchetti A, Angeloni M and Balestrino G 2004 *Eur. Phys. J.* B **37** 339–44